Continuous-wave sum-frequency generation in AlGaAs Bragg reflection waveguides

Junbo Han, Payam Abolghasem, Bhavin J. Bijlani, and Amr S. Helmy*

The Edward S. Rogers Sr. Department of Electrical and Computer Engineering, University of Toronto, 10 King's College Road, Toronto, Ontario M5S 3G4, Canada

**Corresponding author: a.helmy@utoronto.ca*

Received July 24, 2009; revised October 11, 2009; accepted October 16, 2009; posted October 27, 2009 (Doc. ID 114786); published November 20, 2009

Efficient sum-frequency generation in epitaxial GaAs/AlGaAs waveguides is reported. Phase matching is achieved for type II nonlinear interaction using Bragg reflection waveguides. Continuous-wave signal and pump in 1550 nm wavelength window were used for upconversion of photons to the 775 nm region. For a pump and signal with powers of 0.69 mW and 0.35 mW, sum-frequency power of 35 nW was measured. The normalized conversion efficiency was estimated to be 298 % $W^{-1}\,cm^{-2}$ in a device with a length of 2.2 mm. The bandwidth of the process was found to exceed 60 nm. © 2009 Optical Society of America

OCIS codes: 190.5970, 160.4330, 130.3120, 230.1480, 190.2620.

Second-order nonlinearities enable numerous useful frequency conversion processes [1]. Parametric processes such as difference-frequency generation (DFG) are useful in generating long-wavelength coherent radiation in mid-IR regimes, where no laser source exists [2]. Sum-frequency generation (SFG) is also attractive to carry out photon upconversion to the near-IR regime (600–800 nm), where efficient, low-noise, single-photon detectors are present [3,4]. Successful upconversion of telecommunication wavelengths for single-photon detection has been achieved in reverse-proton-exchanged periodically poled lithium niobate (PPLN) waveguides [3] and in z-cut lithium niobate crystals ($LiNbO_3$) [4].

Sum-frequency (SF) devices using compound semiconductors offer distinct benefits. Particularly, devices that are based on the GaAs/AlGaAs material system, which exhibit large second-order nonlinearity ($d_{\mathrm{eff}}^{\mathrm{GaAs}} \approx 100$ pm/V at 1550 nm), broad transparency window (0.9–17 μm), and mature fabrication technology. Despite the aforementioned advantages, phase matching (PM) in compound semiconductors is often challenging owing to lack of natural birefringence and their highly dispersive nature. Recently, we have demonstrated an exact PM technique using Bragg reflection waveguides (BRWs) [5] that utilizes the strong modal dispersion properties of photonic bandgap structures. In this Letter, we demonstrate BRWs as an efficient platform for SFG. The results discussed here are promising for the development of efficient, integrated parametric devices, where the nonlinear components can be monolithically incorporated on the same epitaxial wafer with diode lasers and photodetectors. This results in reducing coupling losses, enhancing detection sensitivity, and ushering the way for integrated optoelectronics for quantum optical applications.

The three-wave mixing of SFG involves the interaction of a pump (p) at wavelength λ_p, a signal (s) at λ_s and the SF wave (i) at λ_i. For an undepleted pump, the power of the SF wave, P_i, can be expressed as [6]

$$P_i = P_p P_s \nu \kappa^2 L^2 \exp[-(\alpha_p + \alpha_s + \alpha_i)\, L/2)] \times \frac{\sin^2(\Delta kL/2) + \sinh^2[(\alpha_p + \alpha_s - \alpha_i)L/4]}{(\Delta kL/2)^2 + [(\alpha_p + \alpha_s - \alpha_i)L/4]^2}, \quad (1)$$

where P_p and P_s are the associated pump and signal powers, ν is the spatial nonlinear overlap factor, L is the waveguide length, $\alpha_j, j \in \{p,s,i\}$ are the propagation losses, and $\Delta k = k_i - k_p - k_s$ is the phase mismatch with k_j taken as the wave numbers of the harmonics. As shown in (1), κ is the nonlinear coupling coefficient defined as

$$\kappa = \left(\frac{8\pi^2 d_{\mathrm{eff}}^2}{n_p n_s n_i c \epsilon_0 \lambda_i^2} \right)^{1/2}, \quad (2)$$

where $n_j, j \in \{p,s,i\}$ are the effective mode indices of the interacting waves, c is the vacuum speed of light, ϵ_0 is the permittivity of free space, and d_{eff} is the effective second-order nonlinear coefficient of the structure. Here, a type II phase matching, where a TM-polarized pump and a TE-polarized signal are mixed to generate a TE-polarized SF wave is explored. Type II interaction was used to benefit from larger d_{eff} in comparison to the type I process. Furthermore, both pump and signal are guided using total internal reflection (TIR), while the SF is a Bragg mode.

Detailed description of the fabricated wafer was previously reported in [7]. The index profile of the structure along with the scanning-electron-microscope (SEM) micrograph of a typical device are illustrated in Figs. 1(a) and 1(b), respectively. The characterized waveguide had a ridge width (W) of 4.4 μm, an etch depth (D) of 3.6 μm, and a device length of 2.2 mm. Also in Figs. 1(c)–1(e) are shown the simulated intensity profiles of the frequencies associated with the type II interaction. From simulation, the effective mode sizes of the pump, signal, and SF were found to be 6.7 μm^2, 6.6 μm^2, and 3.2 μm^2, respectively.

0146-9592/09/233656-3/$15.00

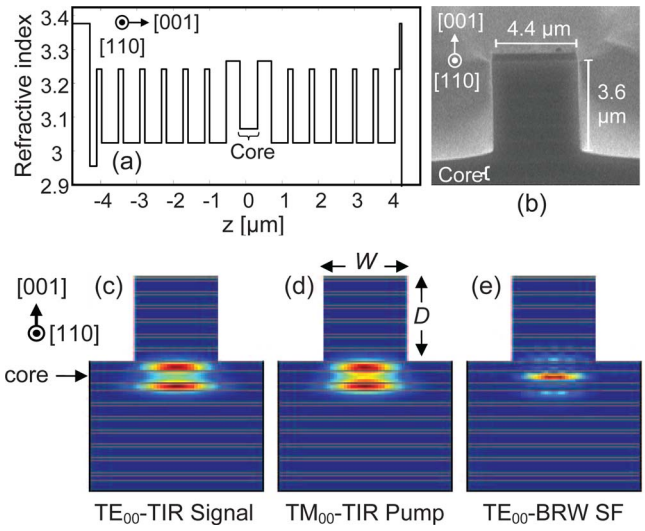

Fig. 1. (Color online) (a) Index profile and (b) SEM of the characterized waveguide [7]. Simulated intensity profiles of (c) TE-polarized signal, (d) TM-polarized pump, and (e) TE-polarized SF. Both pump and signal are TIR modes, while the SF is a Bragg mode.

Using the Fabry–Perot method, linear propagation loss of TM-polarized pump and TE-polarized signal around 1550 nm were measured to be 2.2 cm^{-1} and 2.0 cm^{-1}, respectively. The propagation loss of the SF wave was not measured, as it involves preferentially coupling into the Bragg mode to use the Fabry–Perot method. At the SF the waveguide supports other modes such as the fundamental TIR mode, which would make the Fabry–Perot method measurement challenging to carry out. The Fresnel reflection at the waveguide facets and the input coupling factor due to spatial overlap between the incident beam with the fundamental modes were found to be 29% and 49%, respectively.

The apparatus used to characterize SF generation consisted of two single-mode tunable cw laser sources in the telecommunication wavelength range. The pump and signal were focused into the waveguide using a 40× objective lens. Emerging harmonics from the waveguide output were collected using a 60× microscope objective lens. An IR camera was used for optimizing the coupled beams into the waveguide. The average powers of pump and signal at input/output stages were recorded using InGaAs photodetectors. The average power of the SF signal was monitored using a silicon photodetector. A polarization beam splitter in a TM rejection configuration was used at the output stage to eliminate any existing TM component in the SF signal, hence confirming type II SFG, as well as rejecting the parasitic second-harmonic of TE signal generated in type I interaction.

The SFG tuning curve, which was obtained by monitoring the power of the SF signal as a function of signal wavelength, is illustrated in Fig. 2(a) and is compared with simulations in Fig. 2(b). In obtaining the experimental curve, the average powers of pump and signal were 1.98 mW and 1.00 mW, respectively, measured before the waveguide front facet. Accounting for facet reflection and input coupling factor, internal pump and signal powers were estimated to be 0.69 mW and 0.35 mW, respectively, and maintained fixed over the wavelength sweeping range. From Fig. 2(a), an internal peak SF power of 35 nW was estimated at 1555.1 nm. The fast oscillating component on the spectrum indicates the resonance effects of the waveguide cavity at both signal and SF wavelengths. These resonance effects were also considered in the simulated curves of Fig. 2(b), where the single-pass sum-frequency power of Eq. (1) was multiplied by the Airy function transmission of the signal and SF waves. Simulations indicated that the envelope and fringes of calculated and measured curves agreed best for values of α_i less than 6 cm^{-1}. However, owing to the aforementioned challenges in measuring α_i, these values could not be confirmed experimentally. It should be noted that the low powers used in the experiment ensured the elimination of any third-order nonlinear effects and attest to the efficiency of the process.

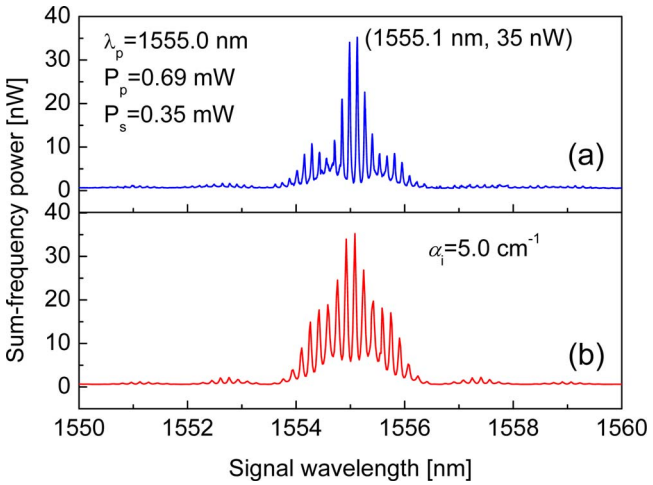

Fig. 2. (Color online) SF power as a function of signal wavelength obtained (a) experimentally and (b) numerically with $\alpha_i = 5.0\ cm^{-1}$. The simulated curves are normalized to the measured peak SF power to facilitate the comparison between the two models.

The quantum efficiency of the device, η_q, is expressed as $\eta_q = P_i\lambda_i/(P_s\lambda_s)$ [4]. The measured quantum efficiency as a function of the pump power is illustrated in Fig. 3 for a signal with 0.35 mW internal

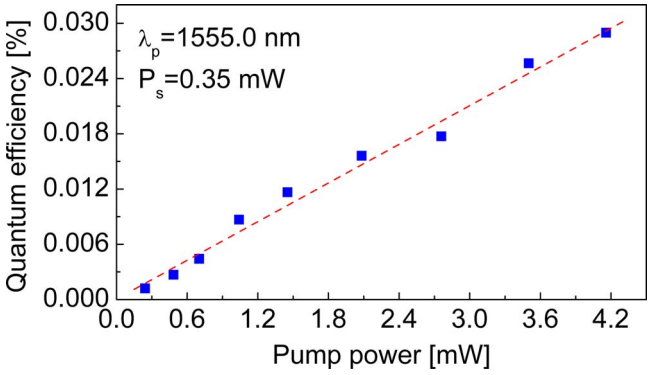

Fig. 3. (Color online) Quantum efficiency as a function of pump power. Squares are the measured data, while the dashed line is the linear fit.

power. One can see that η_q is proportional to the pump power at low power levels. Using the fit in Fig. 3 (dashed line) and a simulated spatial nonlinear overlap coefficient of $\nu=1.14\times10^{-2}\ \mu m^{-2}$, an extracted value of κ was obtained to be $\approx1.60\times10^{-3}\ W^{-1/2}$. The corresponding effective nonlinear coefficient of the structure was then calculated to be $\approx$40 pm/V. Using the model proposed in [8,9], the theoretical d_{eff} of the waveguide was calculated to be 39 pm/V. The close agreement between simulated and extracted d_{eff} is remarkable, since the measured d_{eff} is expected be smaller than the calculated value, given that the expression of η_q does not take into account the propagation losses. Using Eq. (1), at zero detuning where $\Delta k=0$ and neglecting propagation losses, the required pump power for a quantum efficiency of 100% is given by $P_p^{100}=\lambda_s/(\nu\kappa^2L^2\lambda_i)$. The device maximum quantum efficiency was measured to be 0.029%, which was obtained for a pump and signal with internal powers of 4.15 mW and 0.35 mW, respectively. The associated SF power was estimated to be $\approx$0.20 μW. While 100% quantum efficiency can be obtained with a pump power as high as 14 W, other factors such as heat generation and two-photon absorption may further increase this power value. Considering the short waveguide length, this leaves ample room for decreasing P_p^{100} provided that propagation losses can be minimized. For example, P_p^{100} can be reduced to 690 mW for a device length of 10 mm. Another figure of merit that demonstrates the device performance is the normalized SFG efficiency, defined as $\eta_{norm}=P_i/(P_pP_sL^2)$. For our device, η_{norm} was estimated to be 298 % $W^{-1}\,cm^{-2}$ [10]. This suggests that the devices described here have the potential to detect single photons with further optimization, particularly by means of reducing propagation losses.

A salient parameter for an SFG device is the process PM bandwidth. Here, the bandwidth was determined by detuning the pump wavelength from the degenerate wavelength of 1555.0 nm, while the signal wavelength was tuned to maximize the generated SF power. The result is shown in Fig. 4. The large variation in the data was caused by the modulation of Fabry–Perot resonance of signal and SF wave. Broadband phase matching was obtained around 1550 nm with an FWHM bandwidth exceeding 60 nm. The real bandwidth is believed to exceed 60 nm, as the available pump source tunability prevented extension of the wavelength beyond 1600 nm. This feature can be further enhanced through appropriate design of the BRW properties to provide a widely spaced signal and pump with respect to the SF [11]. This will, in turn, facilitate the spectral filtering of parasitic second-harmonic of pump/signal from the SF wave required for practical upconversion applications in integrated single-photon detection [3,4].

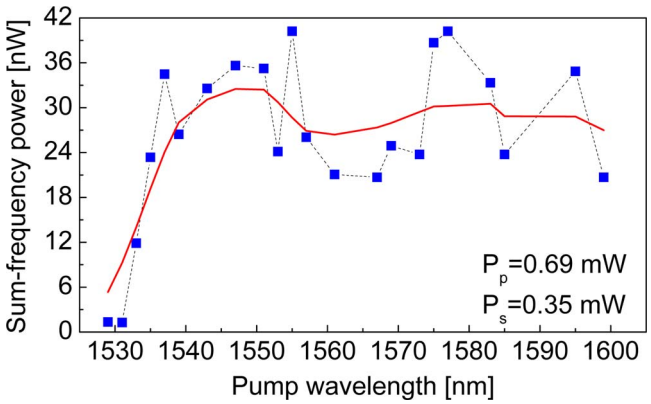

Fig. 4. (Color online) SF power as a function of pump wavelength. Squares are the measured data while the solid-line is a smoothed fit to remove cavity resonance effect. The pump wavelength range limited the tunability on the long wavelength side.

In summary, type II cw SFG with a bandwidth exceeding 60 nm and a normalized conversion efficiency of 298 % $W^{-1}\,cm^{-2}$ using a pump and signal with internal powers of 0.69 mW and 0.35 mW is reported. The device maximum quantum efficiency was estimated to be 0.029%. The high conversion efficiency, the broad process bandwidth, and the possibility of monolithically integration of the waveguide with active elements make the device an attractive candidate for novel integrated optoelectronic circuits such as integrated single-photon counting applications.

This work was supported by the Natural Sciences and Engineering Research Council of Canada (NSERC), Ontario Centres of Excellence (OCE) and Canadian Microelectronics Corporation.

References

1. J. A. Amstrong, N. Bloembergen, J. Ducuing, and P. S. Pershan, Phys. Rev. **127**, 1918 (1962).
2. A. Fiore, V. Berger, E. Rosencher, P. Bravetti, and J. Nagle, Nature **391**, 463 (1998).
3. C. Langrock, E. Diamanti, R. V. Roussev, Y. Yamamoto, and M. M. Fejer, Opt. Lett. **30**, 1725 (2005).
4. M. Fujimura, H. Okabe, K. Beniya, and T. Suhara, Jpn. J. Appl. Phys. **46**, 5868 (2007).
5. B. Bijlani, P. Abolghasem, and A. S. Helmy, Appl. Phys. Lett. **92**, 101124 (2008).
6. R. L. Sutherland, *Handbook of Nonlinear Optics* (Marcel Dekker, 1996).
7. P. Abolghasem, J. Han, A. Arjmand, B. J. Bijlani, and A. S. Helmy, IEEE Photon. Technol. Lett. **21**, 1462 (2009).
8. M. Ohashi, T. Kondo, R. Ito, S. Fukatsu, Y. Shiraki, K. Kumata, and S. S. Kano, J. Appl. Phys. **74**, 596 (1993).
9. I. Shoji, T. Kondo, A. Kitamoto, M. Shirane, and R. Ito, J. Opt. Soc. Am. B **14**, 2268 (1997).
10. R. V. Roussev, C. Langrock, J. R. Kurz, and M. M. Fejer, Opt. Lett. **29**, 1518 (2004).
11. P. Abolghasem, M. Hendrych, X. Shi, J. P. Torres, and M. S. Helmy, Opt. Lett. **34**, 2000 (2009).